Progress In Electromagnetics Research, Vol. 126, 49–64, 2012

PERFORMANCE-OPTIMIZED QUADRATE BOWTIE RFID ANTENNAS FOR COST-EFFECTIVE AND ECO-FRIENDLY INDUSTRIAL APPLICATIONS

Y. Amin[1, *], Q. Chen, H. Tenhunen, and L. R. Zheng

iPack VINN Excellence Center, Royal Institute of Technology (KTH), Stockholm SE-16440, Sweden

Abstract—Fully integrated printed RFID antennas show potential solution for item level labeling applications. In order to accommodate the antenna during the package printing process, it is vastly preferred that antenna structures are printed on paper substrates. However, the electromagnetic properties and thickness of paper substrates are susceptible to change due to various environmental effects. Thus, adequately consistent in performance and material insensitive printed Quadrate Bowtie RFID antennas are proposed. This paper presents an in-depth efficient optimization for high performance tag antenna designs for operability in frequencies 866–868 MHz & 902–928 MHz. It is demonstrated that the proposed antennas can tolerate a considerable variation in the permittivity on thin paper substrates, and present benchmarking results when n across metal and water containing objects.

1. INTRODUCTION

As an ingredient of rapidly emerging technologies in automatic identification and data capture (AIDC) industries, radio frequency identification (RFID) has been increasingly used in many applications such as supply chain management, inventory control, security management, and logistics [1]. To meet the requirements for these applications, RFID tags need to be attached on various objects [2, 3] with different shapes and material properties. Therefore, an RFID tag antenna attached on a target object plays a crucial role in determining the overall performance of an RFID system. Presently much effort is dedicated to the development of RFID antennas by implementing

Received 8 February 2012, Accepted 1 March 2012, Scheduled 8 March 2012

* Corresponding author: Yasar Amin (ysar@kth.se).

Table 1. Substrate parameters evaluated for proposed antennas.

Substrate	Thickness (μm)	Permittivity (ε_r)	Loss Tangent
Kodak Photopaper	280	3.2 (average)	0.077 (1 GHz@25°C)
HP Photopaper	280	3.2 (average)	0.04 (1 GHz@25°C)
Paper (p_e:smart)	250	3.2 (average)	0.077 (1 GHz@25°C)
Metal coated PET	50	3.3	0.003 (0.9 GHz@25°C)

various technologies [4–6]; however, the development area appears deserted while encountering the issues interconnected to the field of economic and eco-friendly tags comprising of paper substrate.

It often overlooked while mentioning the paper printed RFID tags that use of paper defines the entirely new era of electrical performance, which encounters from, new set of issues [7, 8]. The polymer-covered paper substrates have been used to demonstrate electrochemical displays. While these paper coatings compromise the low cost and recyclability, this might still be acceptable for relatively high-value electronic applications that require relatively expensive materials, several processing steps, and encapsulation [9]. Paper substrates offer many advantages for printing RFID antennas, not only is paper widely available and affordable, it is lightweight, biodegradable and can be rolled or folded into 3D configurations [10, 11].

In this paper, novel quadrate bowtie passive RFID tag antennas on paper/PET substrates are presented with the introduction of impedance matching approach to improve the reliability against environmental diversities as well as increase the maximum reading distance. The quadrate bowtie antenna [12] profile modification and T-matching network are used to match the antenna input impedance to tag's chip impedance, and the effects of metal and water on the proposed antennas are also categorically investigated. The European and North American UHF RFID bands are preferred and all simulations are performed using ANSYS HFSS^{TM}. These antennas are printed on different substrates (Table 1) using state-of-the-art printing technologies (**D**ry **P**hase **P**atterning & Inkjet Printing). The measurements are carried out in an anechoic chamber along with the reader setup dedicated to antenna characterization for metal, and water containing objects and proposed antennas are also compared with that of a commercial RFID tag. The ruggedness, eco-friendliness, flexibility and exceptionally long read range of these proposed antennas make them an ideal choice for far-field cases, carton (containing water & metal objects) and (wood or metal) pallet industrial applications.

2. ANTENNA DIMENSIONS AND PARAMETRIC OPTIMIZATION

The proposed quadrate bowtie antennas are optimized on a methodical basis for minimizing the effects of environmental adversities on RFID tags. The main purpose of enhancement is to maximize the feeding power to the load and reduce the antenna area, while realizing the highly efficient structures on paper substrate for eco-friendly tags. Figure 1 shows the Thevenin equivalent circuit of the IC tag, from which the consumption power at the load is evaluated assuming the incident plane waves. In Figure 1, v_o is received open voltage, $Z_a = R_a + jX_a$ the input impedance of the tag antenna, $Z_c = R_c + jX_c$ the impedance of the load, I the current flowing at the load. I and the consumption power of the load P_c are obtained from (1) & (2):

$$I = \frac{v_o}{Z_a + Z_c} \tag{1}$$

$$P_c = Re\{Z_c I I^*\} \tag{2}$$

It is worth mentioning here that throughout the text onwards whenever input impedance of antenna is referred it will be meant that the real part R_a of the antenna input impedance Z_a consists of the radiation resistance and the antenna losses or loss resistance. Hence, one of the optimization criteria is defined as (3),

$$kP_c + \left(1 - \frac{S}{S_{\max}}\right) \rightarrow \max \tag{3}$$

where S is the antenna size and $S_{\max}$ the maximum size, and k in the first term is the weighting constant to offset the first and second terms. If the effect of the second term in the objective function is trivial, the impedance matching between Z_a and Z_c will stand for the optimal antenna, that is, Z_a of the optimized antenna will be the complex conjugate of Z_c. Note that the input voltage v_o depends on the

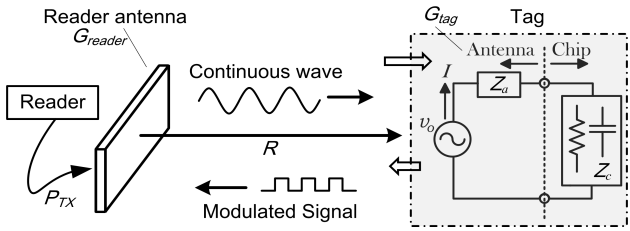

Figure 1. Far-field RFID mechanism & equivalent circuit of an IC tag.

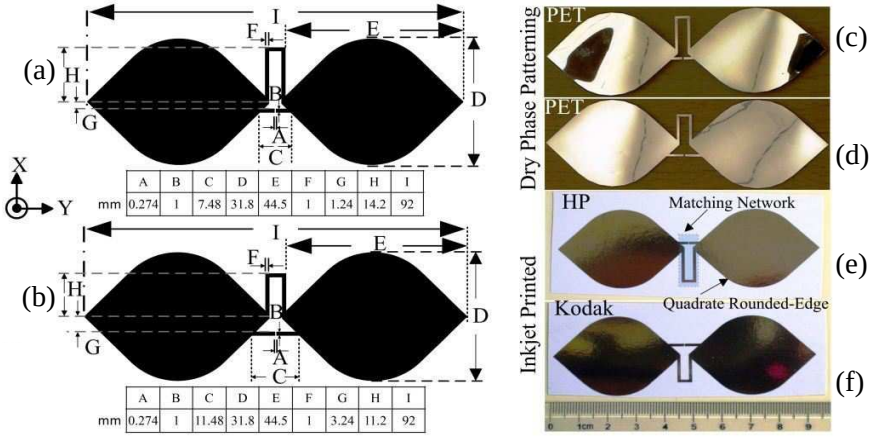

Figure 2. The geometry of RFID antenna for: (a) EU band, (b) NA band; DPP of antenna on PET for: (c) EU band, (d) NA band; inkjet printed antenna on: (e) HP photopaper for EU band, (f) Kodak photopaper for NA band.

antenna structure in this problem [11]. Thus, it requires a conjugate matching technique such as series or parallel stubs. The matching network of the tag has to ensure the maximum power delivered to the chip. To achieve these design goals, a T-matched quadrate bowtie antenna (half wavelength dipole antenna) with rounded corners, is designed and fabricated. This design is used for the matching of the passive antenna terminals to the NXP ucode g2xm (TSSOP8, e.g., the target IC impedance at 915 MHz is 22-j191Ω). The prototype antenna structures for UHF RFID European (EU) band and North American (NA) is shown along with dimensions in Figures 2(a) & (b) respectively. The T-match arms are liable for impedance matching of the antenna terminals to that of the RFID chip through the fine tuning of the series and shunt stubs.

2.1. Antenna Effective Aperture

A commonly disregarded issue about an (RFID) antenna is how directivity and gain are correlated to its physical dimensions. Since the field/current, on the antenna aperture is not uniform, the concept of antenna effective aperture is established to serve this purpose. The effective aperture A_e is less than the physical aperture A_p [13]. The directivity D can also be articulated in expressions of the aperture size

and aperture efficiency η_{ap}:

$$D = \frac{4\pi}{\lambda^2} A_e = \frac{4\pi}{\lambda^2} \eta_{ap} A_p \tag{4}$$

where λ is the wavelength of the radio waves. By knowing the power density S at the receiving antenna, we can approximate the received power P_r:

$$P_r = S A_e \tag{5}$$

Thus during optimization course of action, much effort is devoted to improving the effective aperture to increase the gain while maintaining the low profile of the proposed antennas showed in Figure 2.

2.2. Skin Depth Effect and Antenna Performance

The skin depth and ohmic losses of the printed conductive layer set the boundary conditions for the manufacturing methods, and parameters such as the amount of silver ink and the thickness of the printed layers. Skin depth is one of the significant factors that lead to achieve a certain thickness of the conductive layer/s. Due to the skin effect at high frequencies, e.g., at UHF, the current density is crowded in the region near the surface of a good conductor. More precisely the skin depth is the depth below the surface of the conductor at which the amplitude of the incident electric field decays to 0.37% of the amplitude at the surface of the conductor. Mathematically, the skin depth δ in case of a good conductor is, therefore [13], expressed as:

$$\delta \approx \sqrt{\frac{1}{\pi f \mu \sigma}} \tag{6}$$

where f is the frequency, μ is the permeability and σ is the conductivity of the conductor material. Thus from above we can deduce three key conclusions that surround the manufacturing process of the proposed antennas:

(i) The higher the frequency, (in this particular case, 860–960 MHz), the smaller the skin depth.

(ii) The higher the permeability (in case, it is not that high, which needs attention while printing process), the smaller the skin depth. However for a good conductor, the permittivity has little effect on the skin depth.

(iii) The higher the conductivity (in case, the conductivity of the printed structure is almost 5 times lower than that of bulk silver due to several parametric constrains in manufacturing), the smaller the skin depth.

3. DPP AND INKJET PRINTING: CONDUCTIVE FEATURES

The standard antenna structures for comparison and validation of the concept are fabricated using Dry Phase Patterning (DPP). It is a single step method for patterning metal or polymer layers on most flexible substrates. The laminate of Aluminum (10 μm layer)/PET is patterned for proposed antennas showed in Figures 2(c) & (d) in one single step, unlike in a wet etching process that involves 6–8 steps to achieve the same pattern. Acreo AB has reported patterning resolution of as small as 200 μm and speed up to 150 m/min, which made it a better choice for cost effective RFID tags.

In addition to cutting down on waste and providing an all-in-one substitute to cleanroom deposition technologies, inkjet printing characteristics with regards to accuracy and form make it an exceptionally pleasant contestant for RF circuits. The practicability of inkjet printing for applications at UHF frequencies has been well covered under [9]. The Cabot conductive ink (CCI-300) by Cabot Corp., is used to print these proposed antennas, which contains 19–21% weight of nano-silver particles of less than 20 nm diameter. The large ratio of the area to volume of these nano-silver particles exhibit the significantly lower melting point even less than 100°C. The inkjet printing is carried out utilizing DMP2800 inkjet printer, as showed in Figure 3(a) which is a table-top printer available from Dimatix Inc. To realize substantial RF properties, the printing resolution of 1000 dpi (Dimatix 10 pL cartridge) −2540 dpi (Dimatix 1 pL cartridge) is achieved by adjusting the print head and it is figured out that using this technique a printing resolution of 1000 dpi is suitable for frequencies in the UHF range. Figure 3(b) shows the surface profile of an RFID antenna printed using cartridges jetting out ink droplets. The ink is then jetted at a temperature of 40°C, while the paper substrate mentioned in Table 1 is maintained at 60°C. In all print setups, the substrate is kept at a distance of 0.5 mm from the print head. To ensure reliable RF conductivity, three layers of ink are printed which results in a thickness of around 3 μm while using a heat gun to anneal in between each re-printing cycle.

After printing, the deposited ink also needs to be annealed to ensure adjacent silver nanoparticles in the jetted ink to coagulate with neighbors, allowing for a smoother path for electron flow particularly at high frequencies. Each printed structure is cured in a thermal oven for two hours at 120° resulting into a consistent, measured DC conductivity in the range 9×10^6 [S/m] -1.1×10^7 [S/m]. The conductivity of the printed structure can also be further increased

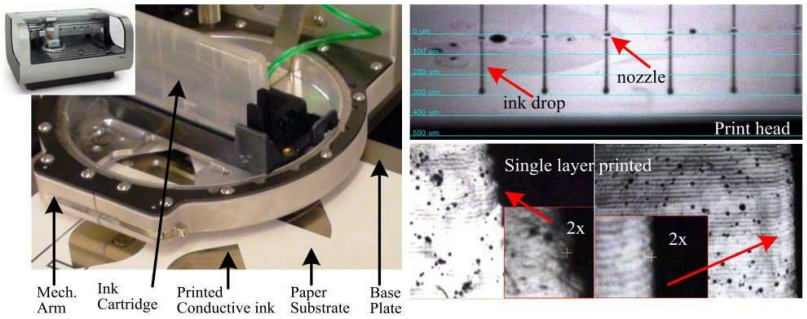

Figure 3. (a) Inkjet printing setup, (b) drop watcher view (top) showing ink printed out of nozzles & images by Fiducial camera of DMP-2800 for inspection of printed ink layer.

by using a higher print resolution setting on the printer. Antenna traces with exceptionally meritorious conductivity and the pitches are accurately fabricated using this inkjet printing process, and is shown by the close-up of a printed trace in Figure 3(b).

4. RESULT ANALYSIS AND DISCUSSION

Passive RFID tags for European and North American UHF RFID bands are manufactured with different substrates mentioned in Table 1, are measured across the frequency band of interest using half mirror method to investigate the reliability aspects of the proposed antennas for commercial grade practices. Ten identical prototypes of proposed structures are manufactured on an each paper substrate in order to determine the worst case analysis ingredients. Thus, each curve in Figure 4 represents the highest deviated values at a certain point among identical samples.

Impedance measurements are taken using vector network analyzer (MS2026B, Anritsu). The standard calibration procedure short-open-load (SOL) is adopted for accuracy of results. In order to verify the performance of the inkjet printed antennas of Figures 2(e) & (f), measurements are also executed using standard antenna prototypes fabricated on Aluminum coated PET substrate as showed in Figures 2(c) & (d). These standard prototypes have the same dimensions as that of proposed antennas and are fabricated using DPP (Dry Phase Patterning) process at Acreo AB. The impedance variation of antenna in Figure 2(a) is shown in Figures 4(a) & (b). Whereas, input impedance plots of antenna in Figure 2(b) are shown

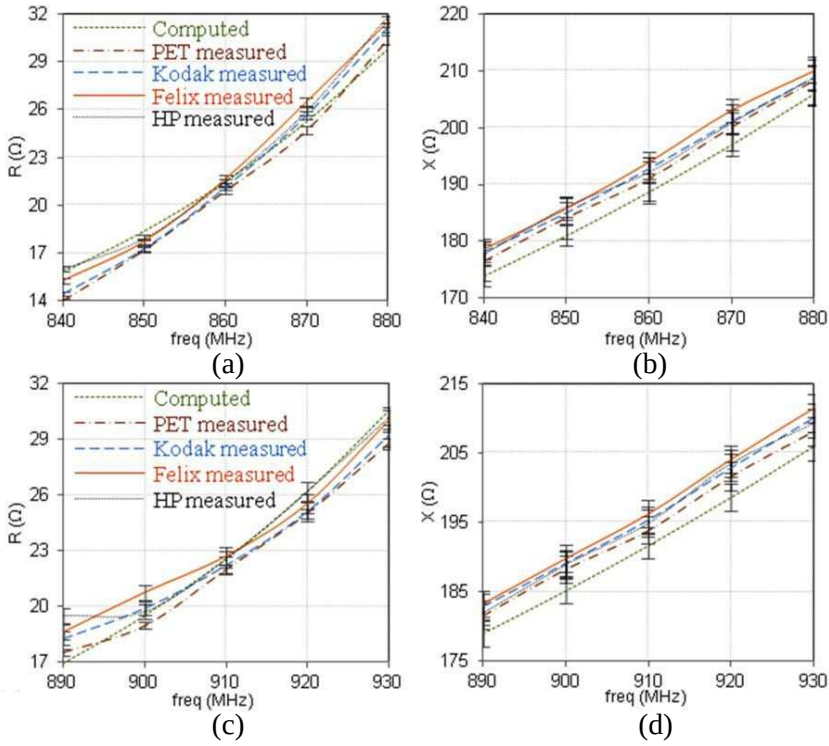

Figure 4. EU band's antenna input: (a) (radiation & loss) resistance variation, (b) reactance variation; NA band's antenna input: (c) (radiation & loss) resistance variation, (d) reactance variation.

in Figures 4(c) & (d). The resistive parts of impedance as showed in Figures 4(a) & (c) for EU and NA band antennas respectively, printed on different photopapers demonstrate consistency to the DPP antennas & simulated results throughout frequency band of interest which is a primary concern for antennas stable behavior. However, slightly greater drift is observed in the resistive part of the antennas printed on paper (p_e:smart) from Felix Schoeller as compared to the others but the difference remains within the acceptable range. Similarly, fairly coherent trend of reactance curves is depicted in Figures 4(b) & (d) for both proposed structures. The formation of round corners is used to obtain wider impedance band. Round corners at the sharp vertexes decreases the reflection of incident current near the edges and changes the current distribution on radiation surfaces. Thus, flatter impedance within the frequency band of interest with much stable real

and imaginary parts is demonstrated in Figure 4.

Using the Friis equation, the read range which is one of the most dominant tag performance characteristics can be estimated by Equation (7) defining forward-link-limited range and Equation (8) defining reverse-link-limited range. Read range is also susceptible to the tag orientation, the object which the tag is placed on, path loss, spatial and temporal fading statistics of the propagation environment [14].

$$R_{forward} = \left(\frac{\lambda}{4\pi}\right)\sqrt{\frac{P_{TX}G_{reader}G_{tag}}{P_{\min,tag}}} \tag{7}$$

and defining the minimum signal power for demodulation at the reader as $P_{\min,rdr}$ we obtain the reverse-link-limited range:

$$R_{reverse} = \left(\frac{\lambda}{4\pi}\right)\sqrt[4]{\frac{P_{TX,reader}T_bG_{reader}^2G_{tag}^2}{P_{\min,rdr}}} \tag{8}$$

where the output power of the reader is P_{TX}, the gain of the reader antenna is G_{reader}, and the gain of the tag antenna is G_{tag}. λ is the wavelength in free space at the operating frequency, $P_{\min}$ is the minimum power required to turn on the tag chip and T_b is backscatter transmission loss.

The read range from Equations (7) & (8) gives the maximum distance at which RFID reader can interpret the tag in free space. Thus, this statement of read range is invalid at near-field distances. In the near-field region, the E and H-fields are not orthogonal so anything within this region couples with the antenna and distort the pattern; thus, the antenna gain is not a valid parameter here. Therefore, the near-field performance testing is carried out inside the anechoic chamber with Impinj's UHF RFID reader kit. The far-field distance is calculated by $(2D^2/\lambda)$, and it is observed as an estimate because the transition from near-field to far-field is not instantaneous. The D (maximum dimension of the radiating structure) of the reader antenna used is 0.3 m (1foot), thus in measurements which are taken at 915 MHz ($\lambda = 0.33$ m) the far-field distance is estimated to be 0.56 m. The proposed antennas exhibit superior readability within reactive near-field region. It is observed that, in the near-field region the antenna pattern is taking shape but is not fully formed, and the antenna gain measurements vary with distance.

In most UHF RFID systems, the reading distance obtained by Equations (7) & (8) extends well into the far-field region. When there is an implementation of tag which can operate in the far-field also involves near-field tag scanning. It can be expected that, in almost all

cases, the tag gets more than sufficient power to operate when brought closer to RFID reader antenna. Hence, the read range of most UHF RFID tags is determined by the tag working in the far-field [15]. The proposed antennas have surpassed read range from 6.5 m (HP) – 7.0 m depending upon which substrate is utilized. Furthermore, the detailed analysis of read range variation is presented in Tables 2 & 3.

The return loss results of antennas in Figures 4(a) & (b) is shown in Figures 5(a) & (b) respectively. It is pragmatic that the return loss of the inkjet printed antennas is slightly higher than the return loss of standard PET substrate antennas. Overall, good agreement between the standard PET-based, and the inkjet printed antennas is observed, regardless of the higher metal loss of the silver based conductive ink. The distortion is possibly due to the effect of metal ground fixture used for half mirror method [16].

The most challenging in measurement steps, the radiation pattern of antennas is measured in an anechoic chamber setup that replicate absolute free space which is presented in Figure 6. The antenna under test (AUT) is mounted over the positioner assembly in the

Table 2. Analysis of effect by metal on the proposed tag at 915 MHz.

Measured → • Computed → ∗	Input impedance (Ω)•	Radiation efficiency (%)∗	Trans. coeff. (dB)∗	Directivity (dBi)∗	Gain (dBi) ∗	Reading range, R (m)•
Free space	24.42 + j194.92	83.64	−1.07	1.85	1.97	6.50
$d = 1$ mm	4.31 + j152.13	1.02	−13.57	7.96	−10.37	0.31
$d = 5$ mm	5.76 + j173.06	6.61	−9.97	8.26	−1.12	1.14
$d = 10$ mm	7.75 + j186.55	18.02	−3.53	8.29	0.58	3.22
$d = 15$ mm	10.17 + j193.10	30.67	−0.67	8.28	2.92	8.10

Table 3. Analysis of effect by water on the proposed tag at 915 MHz.

Measured → • Computed → ∗	Input impedance (Ω)•	Radiation efficiency (%)∗	Trans. coeff. (dB)∗	Directivity (dBi)∗	Gain (dBi)∗	Reading range, R (m)•
Free space	24.42 + j194.92	83.64	−1.07	1.85	1.97	6.50
$d = 1$ mm	129.27 + j330.00	8.77	−9.51	4.12	−7.51	0.61
$d = 5$ mm	23.61 + j201.20	6.29	−1.32	2.67	−10.05	1.15
$d = 10$ mm	13.77 + j189.04	20.26	−0.33	2.81	−3.02	3.23
$d = 15$ mm	12.20 + j189.90	27.64	−0.15	3.73	−1.13	4.37
$d = 20$ mm	10.21 + j190.82	38.31	−0.08	4.93	−0.12	5.26

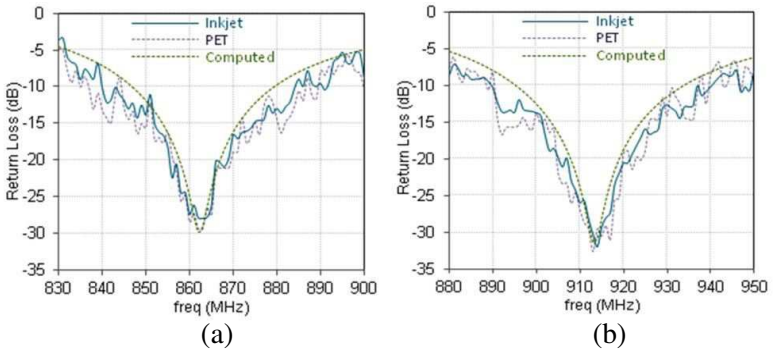

Figure 5. Return loss of antennas for: (a) EU band, (b) NA band.

Figure 6. The anechoic chamber & instruments used.

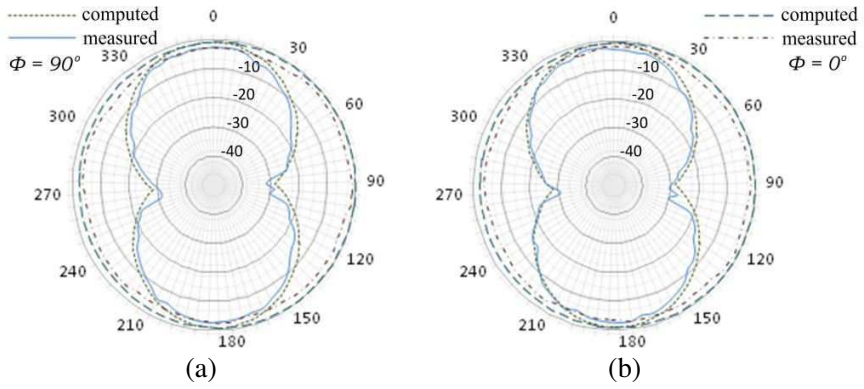

Figure 7. Measured & computed 2D far-field radiation plots of antennas for: (a) EU band, (b) NA band.

center of the chamber which is set to rotate the antenna in small steps of 5 degrees to obtain a 360° radiation pattern. A continuous-wave (CW) signal from the signal generator excites the AUT. The receiver antenna is connected to the spectrum analyzer (Agilent HP 8562E) and a PC running the test automation software controls the measurement setup. Soft soldering is avoided to fix the AUT to the test fixture since it requires heating the filler metal above 250°C to achieve proper soldering, but this temperature severely damages the printed traces on paper substrates. Thus, antennas are attached to the test terminal with CW2400 silver conductive epoxy, cured at 24°C for 4 hours to reach maximum conductivity and adhesion. The normalized computed radiation pattern and the microwave chamber measurements are plotted in Figure 7. The radiation patterns are nearly uniform (omnidirectional) at 915 MHz. They show remarkably satisfactory agreement between computations and measurements. The same uniformity in antenna radiation pattern could be demonstrated for other frequencies within the antenna's bandwidth. Similar parametric behavior is depicted by proposed antennas for EU band, which are shown in Figures 2(a), (c) & (e).

5. ANALYSIS FOR INDUSTRIAL APPLICATIONS

5.1. Effects of Metal on Tag Antenna Performance

The metal effect is limited in the tag antenna which has its own ground plane [17, 18]. However, the antenna which does not have a ground plane, such as quadrate bowtie, the radiation characteristics and input impedance of the antenna, are distorted when the tag is placed on or near a metal object. Whenever there is an encounter with metal objects these variations certainly impact the tag performance [5]; however, even if it is not possible to eliminate it completely [3]; it is made possible in the proposed antennas to, strongly limit this phenomenon.

The comprehensive data on the metal effect on the proposed RFID tag antenna placed close to a metal plate and reading distance at 915 MHz is summarized in Table 2. The antenna is positioned parallel to and below a metal plate measuring 30 cm × 30 cm. The directivity, radiation efficiency, gain, and input impedance, are examined for the different distances from the metal plate. Considering the worst case, i.e., when the antenna is placed extremely close to the metal plate ($d = 1$ mm), the directivity of the antenna enhances significantly to around 8 dBi. However, the radiation efficiency plunges drastically to 1.02%, which results in remarkably low gain of −10.37 dBi at 915 MHz. Particularly, the real part of the input impedance varies severely, as well. This variation in impedance outcome in deprived impedance

matching with the RFID tag chip (circuit showed in Figure 1), resulting in a transmission loss of −13.57 dB at 915 MHz. The gain reduction and poor impedance matching results in the reading distance reducing to 0.31 m. However, the proposed antenna still exhibited superior reading distance when placed so closer to the metal object in coherence with previously published results [3, 18].

The directivity of the antenna remains virtually unchanged, by moving the antenna further away from the metal plate. In the meantime, the radiation efficiency shows an escalating drift, which domino result in increasing antenna gain. The real part of the input impedance shows modest change, whereas the imaginary part inclined to values close to those in free space. An increasing trend is observed in the reading distance; when the tag is moved away from the metal plate. When the tag is moved to $d = 5$ mm, the reading distance exhibits higher value than that of in free space because the metal plate acts as a reflector which ultimately boosts the tag antenna gain. In conclusion, although the metal object degrades the reading range of the tag significantly when it is directly attached or is placed real close to it, but the proposed antennas are even capable of reasonably communicating under these critical testing conditions.

5.2. Effects of Water on Tag Antenna Performance

Table 3 shows the complete characteristic analysis of the proposed antenna which is placed close to a water cuboid. The antenna is placed parallel to and above a water cuboid which is measuring 30 cm × 8 cm × 8 cm; whereas, $\varepsilon_r = 77.3$ and $\delta \tan = 0.048$ [19] of water is adopted in this experimentation. The input impedance, radiation efficiency, directivity, and gain are inspected at different distances away from the water cuboid. When the proposed antenna is placed closer to water at a distance of $d = 1$ mm, the directivity of the antenna amplifies while the radiation efficiency reduces considerably, which domino effect in a decrease, in the antenna gain.

In dissimilarity with the metal plate effect, it is pragmatic that the water always causes a decrease in the gain regardless of the distance between the water and the proposed antenna. When the antenna is moved further away at a distance of $d = 15$–20 mm, the antenna gain achieves the value roughly equal to that in free space. The input impedance displays a smoother variant with the exception of the situation once the antenna is extremely close to the water, i.e.; $d = 1$ mm. If the tag antenna is placed extremely close to water (that means almost touching the cuboid), the reading distance reduces considerably to 0.61 m but not that much as observed in the case of metal plate. When the tag is moved further away, the effect of the

water is declined; resulting in read range enhancement. Therefore, exhibiting the graceful degradation in functionality for suitability in high performance industrial applications. The proposed antennas exhibit improved performance and are in accordance with commercially available RFID tags and previously published results [20].

Furthermore, the metallic plate and water do not degrade the bandwidth of the proposed antennas to such an extent that they become unreadable until the tag is placed closer than $d = 1\,\text{mm}$. The bandwidth degradation behavior is constant, in case the tag is brought nearer to the water containing objects, but in case of metallic plate, the bandwidth degradation is more serious particularly within $d = 5\,\text{mm}$. The proposed antennas are designed with reasonably wideband in order to demonstrate readable bandwidth at the expense of read range (bandwidth vs. read range trade-off) which limits their usage to narrow bandwidth operations, i.e., either for EU band or NA band. The stabilization of bandwidth can further be achieved by reducing the effect of matching network, but that will induce instability against dielectric variation of paper substrate, so it is trade-off always among optimum values depending upon the applications.

6. CONCLUSION

The novel quadrate bowtie antennas for UHF RFID industrial applications have been proposed and fabricated on paper and PET substrates, using inkjet printing and DPP technology respectively. In addition to categorical optimization of antenna profile, a T-matching network is introduced to develop a novel compact, RFID tag, featuring outstanding overall performance. The antennas exhibit exceptional operational characteristics when stumble upon metal and water containing objects. The use of the inkjet printing process in the development of these proficient RFID antennas on different types of paper has also been demonstrated, verifying that paper-based inkjet printing topologies offer a remarkably low-cost, "green" solution to system-level packaging for UHF, wireless, and microwave applications.

ACKNOWLEDGMENT

The author would like to thank Peter Fuks in school of electrical engineering at KTH who generously provided measurement facilities. This work was financially supported by Vinnova (The Swedish Governmental Agency for Innovation Systems) through the Vinn Excellence centers program and by the EU project CLIP of grant number 243557 through EU FP7-SME-2008-2.

REFERENCES

1. Zuo, Y., "Survivable RFID systems: Issues, challenges, and techniques," *IEEE J. SMCC*, Vol. 40, No. 4, 406–418, 2010.
2. Tiang, J.-J., M. T. Islam, N. Misran, and J. S. Mandeep, "Circular microstrip slot antenna for dual-frequency RFID application," *Progress In Electromagnetics Research*, Vol. 120, 499–512, 2011.
3. Chen, S.-L., S.-K. Kuo, and C.-T. Lin, "A metallic RFID tag design for steel-bar and wire-rod management application in the steel industry," *Progress In Electromagnetics Research*, Vol. 91, 195–212, 2009.
4. Panda, J. R. and R. S. Kshetrimayum, "A printed 2.4 GHz/5.8 GHz dual-band monopole antenna with a protruding stub in the ground plane for WLAN and RFID applications," *Progress In Electromagnetics Research*, Vol. 117, 425–434, 2011.
5. Hsu, H.-T., F.-Y. Kuo, and C.-H. Chang, "Application of quasi log-periodic antenna for UHF passive RFID tag design featuring constant power transmission coefficient over broadband operation," *Journal of Electromagnetic Waves and Applications*, Vol. 24, Nos. 5–6, 575–586, 2010.
6. Jamlos, M. F., T. A. Rahman, M. R. Kamarudin, P. Saad, M. A. Shamsudin, and A. M. M. Dahlan, "A novel adaptive Wi-Fi system with RFID technology," *Progress In Electromagnetics Research*, Vol. 108, 417–432, 2010.
7. Alimenti, F., M. Virili, G. Orecchini, P. Mezzanotte, V. Palazzari, M. M. Tentzeris, and L. Roselli, "A new contactless assembly method for paper substrate antennas and UHF RFID chips," *IEEE Transactions on Microwave Theory and Techniques*, Vol. 59, No. 3, 627–637, 2011.
8. Lazaro, A., D. Girbau, and R. Villarino, "Effects of interferences in UHF RFID systems," *Progress In Electromagnetics Research*, Vol. 98, 425–443, 2009.
9. Tobjërk, D. and R. Österbacka, "Paper electronics," *Adv. Mater.*, Vol. 23, No. 17, 1935–1961, 2011.
10. Bose, I. and S. Yan, "The green potential of RFID projects: A case-based analysis," *IEEE IT Pro.*, Vol. 13, No. 1, 41–47, 2011.
11. Makimura, H., Y. Watanabe, K. Watanabe, and H. Igarashi, "Evolutional design of small antennas for passive UHF-band RFID," *IEEE J. MAG*, Vol. 47, No. 5, 1510–1513, 2011.
12. Qu, S.-W. and C.-L. Ruan, "Effect of round corners on bowtie antennas," *Progress In Electromagnetics Research*, Vol. 57, 179–

195, 2006.

13. Huang, Y. and K. Boyle, *Antennas from Theory to Practice*, John Wiley & Sons Ltd., New York, 2008.
14. Nikitin, P. V. and K. V. Rao, "Antennas and propagation in UHF RFID systems," *IEEE International Conference on RFID*, 277–288, 2008.
15. Tikhov, Y., "Comments on 'antenna design for UHF RFID tags: A review and a practical application," *IEEE J. AP*, Vol. 54, No. 6, 2006.
16. Kuo, S.-K., S.-L. Chen, and C.-T. Lin, "An accurate method for impedance measurement of RFID tag antenna," *Progress In Electromagnetics Research*, Vol. 83, 93–106, 2008.
17. Sanchez-Montero, R., S. Salcedo-Sanz, J. A. Portilla-Figueras, and R. Langley, "Hybrid pifa-patch antenna optimized by evolutionary programming," *Progress In Electromagnetics Research*, Vol. 108, 221–234, 2010.
18. Lin, D. B., I.-T. Tang, and C.-C. Wang, "UHF RFID H-shaped tag antenna using microstrip feed design on metallic objects," *Journal of Electromagnetic Waves and Applications*, Vol. 25, No. 13, 1828–1839, 2011.
19. Xi, J., H. Zhu, and T. T. Ye, "Platform-tolerant PIFA-type UHF RFID tag antenna," *International IEEE Conference on RFID*, 174–180, 2010.
20. Bjorninen, T., A. Z. Elsherbeni, and L. Ukkonen, "Low-profile conformal UHF RFID tag antenna for integration with water bottles," *IEEE J. AWPL*, Vol. 10, 1147–1150, 2011.